Subdiffraction Focusing Metalens Based on the Depletion of Bessel Beams

Yu Li, Xinhao Fan 🆔, Peng Li, and Jianlin Zhao

Abstract—**Superresolution microscopy is of great interests in modern optics and photonics applications. Subdiffraction focusing lens, that has superresolution focal spot with local spatial frequency greater than the maximum Fourier component, has attracted intensive attentions in past decade, because of the significant capability of unlabeled far-field superresolution. Here, we propose a dielectric subdiffraction focusing metalens based on the depletion of Bessel beams. Different from traditional binary wavefront modulation elements, this metalens is designed according to the reverse engineering of subdiffraction focal field, which is constructed from the depletion of a fundamental Bessel beam. With the independent amplitude and phase control ability of dielectric metasurface, this metalens enables breaking the diffraction limit and can produce a focal spot with full width at half maximum of 0.3λ/NA. This work may provide a platform for the design of integrated and compact photonic devices to control the light propagation dynamics and spin angular momentum associated with circular polarization.**

Index Terms—**Metalens, subdiffraction focusing, bessel beam, polarization.**

I. INTRODUCTION

DEVELOPING the focusing technology that overcomes the theoretical limit is always a hot research spot in the fields of optics and photonics. Numerous milestone technologies with subdiffraction resolution such as near field optical scanning microscopes [1], stimulated emission depletion [2], and surface enhanced Raman scattering [3], have been proposed, greatly facilitating the development of optical imaging. In contrast to these approaches, the label-free superresolution focusing in the far field is more significant both in living imaging and elaborate processing [4]–[6].

Superoscillation is a typical phenomenon that refers to local frequency in a band-limited signal oscillating greater than the maximum frequency [7]. In optical realm, Berry and Popescu first introduced and pointed out that light field diffracted through subwavelength grating can produce arbitrarily small spatial energy region [8]–[11], that is, optical superoscillation. In 2007, Zheludev first experimentally observed this typical phenomenon by using metallic nanohole array with quasiperiodic structure [12]. Subsequently, series of optical devices dedicated to improving superoscillation performance have been proposed [13]–[22]. For instance, metallic and dielectric masks composed of concentric rings with binary amplitude and phase combined masks with higher efficiency [23], as well as optical fibers with complex amplitude modulation structure at the end [24]–[26]. Recently, the rapidly developed metasurfaces, which enable the simultaneous modulation of polarization, amplitude, and phase of wavefront in a subwavelength scale [27]–[29], brings new opportunities for the development of superoscillating light field [30]–[35], because of the multiple parameter modulation capability [36]–[41].

In this paper, we propose a dielectric subdiffraction focusing metalens based on the Bessel function modulation method, to generate superoscillating focal spot. We use the modulated first order Bessel beam with opposite phase to deplete the fundamental order one, and obtain the complex amplitude function of the spectral space mask through Fourier transform after iteration algorithm. With the independent amplitude and phase control ability of dielectric metasurface, we design and fabricate dielectric metalens that can break the diffraction limit. The focal spot generated by the designed dielectric metalens is achieved to 0.3λ/NA.

Yu Li is with the Key Laboratory of Light Field Manipulation and Information Acquisition, Ministry of Industry and Information Technology, Xi'an, Shaanxi 710129, China, with the Shaanxi Key Laboratory of Optical Information Technology, School of Physical Science and Technology, Northwestern Polytechnical University, Xi'an, Shaanxi 710129, China, and also with the Xi'an Ming De Institute of Technology, Xi'an, Shaanxi 710124, China (e-mail: liyu@mdit.edu.cn).

Xinhao Fan, Peng Li, and Jianlin Zhao are with the Key Laboratory of Light Field Manipulation and Information Acquisition, Ministry of Industry and Information Technology, Xi'an, Shaanxi 710129, China, and also with the Shaanxi Key Laboratory of Optical Information Technology, School of Physical Science and Technology, Northwestern Polytechnical University, Xi'an, Shaanxi 710129, China (e-mail: pengli@nwpu.edu.cn; 2018202354fanxinhao@mail.nwpu.edu.cn; jlzhao@nwpu.edu.cn).

Digital Object Identifier 10.1109/JPHOT.2022.3144398

II. THEORY AND RESULTS

Fig. 1 illustrates the basic principle of the melalens. As shown, a circularly polarized light field normally illuminates the metalens, whereby the output field under complex amplitude modulation generates a subdiffraction focal spot in the focal field. Considering the diffraction property of a circular aperture [42]–[45], we utilize the Bessel function to design the mask [35], [40], [46], of which the complex amplitude modulation function is generated by the iteration algorithm shown in Fig. 2.
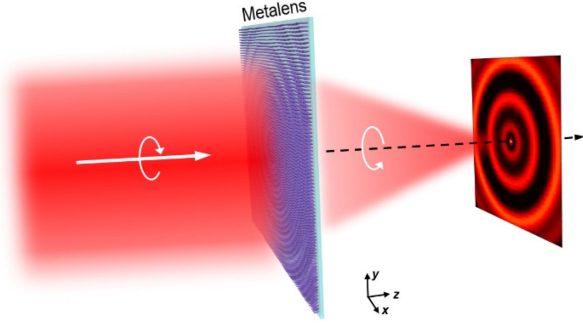
Fig. 1.   Schematic illustration of the subdiffraction focusing metalens.

Fig. 2.   Iteration algorithm of the complex amplitude of the mask.

Fig. 3.   (a), (b) Transmission amplitude distributions of the mask and optimized metalens, respectively. (c), (d) Radial distributions of transmission amplitude and phase of the metalens. (e), (f) Intensity distributions of focal fields corresponding to the maximum frequency and targeted focal field, respectively. (g) Comparison of radial intensity distributions.
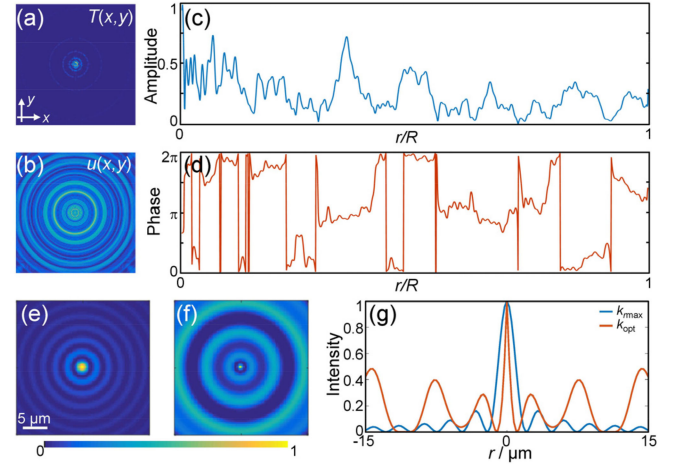
We first suppose that the focal field presents a fundamental order Bessel function distribution of $J_0(k_{r0}r)$, with k_{r0} is the transverse wave vector component that determines the size of the central bright spot. Then, to deplete the central spot, we coaxially overlap a first order Bessel beam with identical transverse wave vector but inverse phase, i.e., $J_1(k_{r0}r)e^{i\pi}$. In this case, the central bright spot of the superposition field can be regarded as another fundamental order Bessel functional spot, whose transverse wave vector is equivalent to k_{r1}, i.e., $E(k_{r1}, r) \propto J_0(k_{r0}r) + J_1(k_{r0}r)e^{i\pi}$. Supposing that the numerical aperture (NA) of the system has a maximum transverse wave vector component $k_{r\max}$, if the effective transverse wave vector of the nth iteration is smaller than $k_{r\max}$, i.e., $k_{rn} < k_{r\max}$, another first order Bessel beam with effective transverse wave vector k_{rn} but inverse phase is introduced again to deplete the central spot.

According to the iteration algorithm, we construct a targeted focal field $E(x,y)$ presenting subdiffraction focus, whose size is smaller than the focal spot corresponding to the maximum spatial frequency. We then generate the spatial frquency mask by the Fourier transform, whose complex amplitude is described as $T(x,y) = \mathscr{F}^{-1}\{E(x,y)\}$. Fig. 3(a) displays the transmission amplitude distribution of the mask. To simplify the system, we design a compact metalens combining the proformances of mask and Fourier transform lens [47]. In this principle, the complex amplitude of the mask is replaced by a transfer function that contains the propagation process from the front focal plane to the surface of lens, which can be described as the diffraction of spatial frquency mask as follow

$$U(x,y) = u(x,y)\,e^{i\varphi(x,y)}$$
$$\propto \mathcal{F}\left\{ \frac{1}{2\pi k_z}\mathcal{F}^{-1}\left\{E(z)\exp(ik_{z0}z)\right\}\exp\left(ik\frac{x_0^2+y_0^2}{2f}\right)\right\}, \quad (1)$$

where, $u(x,y)$ and $\varphi(x,y)$ are the transmission amplitude and phase of the metalens, respectively, and f depicts the focal length. Fig. 3(b) displays the transmission amplitude distribution of the metalens, and Figs. 3(c) and 3(d) show the radial distributions of tranmsission amplitude and phase.

For the sake of experimental observation, the aperture and focal length of the mentalens are selected as $D = 1$ mm and $f = 4$ mm. Thus, NA $= 0.124$, the maximum transverse wave vector is $k_{r\max} = $ NA$\cdot k_0 = 1.16 \times 10^6$ m^{-1}. In the iteration process, the initial transverse wave vector component is defined as $k_{r0} = 0.004k_0 = 37523$ m^{-1}. In such a case, the targeted focal field can be expressed as $E(r) = J_0(k_{r0}r) + \Sigma J_1(k_{rn}r)e^{i\pi}$, with iteration number $n = 5$. The total transmission of this mask is 17.9%. Figs. 3(e)-3(g) compares the focal field intensity distributions corresponding to the maximum frequency and the targeted focal field. From the radial intensity distribution diagram, i.e., Fig. 3(g), one can find that, the full width at half maximum (FWHM) of the focal spot corresponding to the maximum frequency is about 2 μm, while for the metalens designed by our method, the FWHM of the focal spot is about 0.95 μm, which obviously produces the superoscillating focusing phenomenon.

III. EXPERIMENT AND RESULTS

We selected the polycrystalline silicon (Poly-Si) to design and fabricate the metalens [48], of which the meta-atom is schematically shown in the inset of Fig. 4(a). This meta-atom consists of a SiO$_2$ substrate and Poly-Si rectangular nanopillars. According to the effective waveguide theory, the Jones matrix
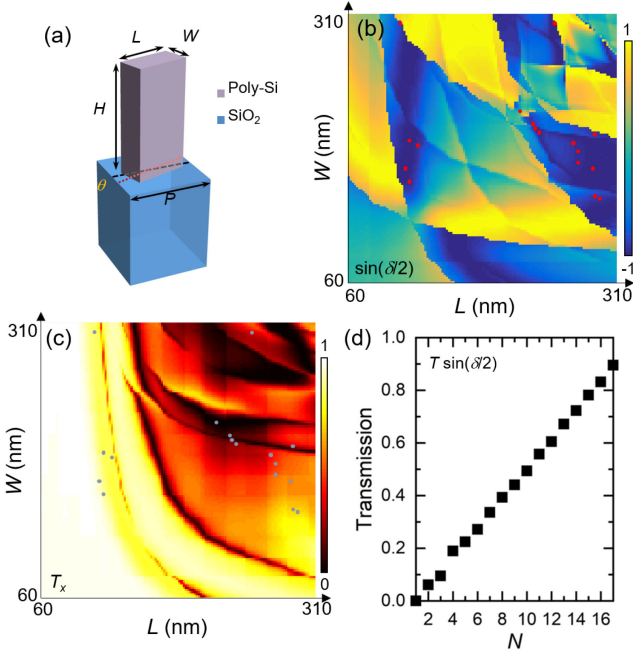
Fig. 4. (a) Schematic geometry of the dielectric meta-atom. Simulated (b), (c) phase retardations $\sin(\delta/2)$ and transmission amplitude T_x vs. the geometric sizes (L and W depict the length and width) of nanopillar at the wavelength of 670nm, respectively. The height and period of the nanopillar are 570nm and 450nm, respectively. The red and gray points in two graphs depict the geometric sizes of these selected structures. (d) Combined transmission amplitudes $T\sin(\delta/2)$ of these selected geometries.

corresponding to this meta-atom can be expressed as [28]

$$\mathbf{J} = R(-\theta)$$
$$\begin{bmatrix} T_x e^{i\varphi_x} & 0 \\ 0 & T_y e^{i\varphi_y} \end{bmatrix} R(\theta), \quad R(\theta) = \begin{bmatrix} \cos\theta & \sin\theta \\ -\sin\theta & \cos\theta \end{bmatrix} \quad (2)$$

where, θ depicts the rotation angle of the rectangle nanopillar, $T_{x,y}$ and $\varphi_{x,y}$ are the amplitude and phase of the transmitted field associated with two eigenstates, which oscillate along the long and short sides of the rectangle geometry, respectively. Here we set $T_x = T_y = T$, and the Jones matrix thus can be expressed as

$$\mathbf{J} = T e^{i\varphi_0} \begin{bmatrix} \cos\frac{\delta}{2} + i\sin\frac{\delta}{2}\cos(2\theta) & i\sin\frac{\delta}{2}\cos(2\theta) \\ i\sin\frac{\delta}{2}\cos(2\theta) & \cos\frac{\delta}{2} - i\sin\frac{\delta}{2}\cos(2\theta) \end{bmatrix} \quad (3)$$

where $\delta = \varphi_x - \varphi_y$ and $\varphi_0 = (\varphi_x + \varphi_y)/2$. For the incidence of a circularly polarized field, whose polarization is described as $E_0[1\ i]^T$, the output field can be expressed as

$$E_{out} = \frac{E_0 e^{i\varphi_0}}{\sqrt{2}} T \cos\frac{\delta}{2} \begin{bmatrix} 1 \\ i \end{bmatrix} + i\frac{E_0 e^{i\varphi_0}}{\sqrt{2}} T \sin\frac{\delta}{2} e^{i2\theta} \begin{bmatrix} 1 \\ -i \end{bmatrix}. \quad (4)$$

Equation (4) clearly shows that, the output field consists of two components with orthogonal circular polarizations. The first one, namely, the directly transmitted component, has the same polarization with the incident field. The second component has opposite polarization, whose complex amplitude can be expressed as $E_0 T \sin(\delta/2)\exp[i(\varphi_0 + 2\theta)]$. That is, the amplitude and phase of this component are determined by T, δ and φ_0, 2θ, respectively [47]. As thus, both the amplitude and phase can be completely and independently controlled. We note that the focal length is too small to inset a circular polarization filter. Therefore, the co-axially directly transmitted component, i.e., the first term in the right side of Eq. (4), should be inherently eliminated. So we set $\delta = \pm\pi$, thus $\cos(\delta/2) \equiv 0$. In such a special case, $\sin(\delta/2) \equiv \pm 1$, that is, the meta-stom works as a half-wave plate, by which the incident polarization can be totally transformed into the opposite one with transmission complex amplitude expressed as $E_0 T \exp[i(\varphi_0 + 2\theta)]$. Obviously, the amplitude of the output field is only dependent on the transmission of the meta-atom, which is determined by the geometric size. While, the phase function is related to the combination of propagation and geometric phases, i.e, φ_0 and 2θ. To break this correlation, here we introduce an indirect parameter, which is defined as $\theta' = \theta - \varphi_0/2$, this means that we can eliminate the propagation phase by adding an opposite rotation angle of $\varphi_0/2$. Therefore, the output light field from each meta-atom has independently controllable amplitude and phase, which are tunable by selecting the geometric size and orientation angle of the nanopillar, respectively.

According to this principle, we select 17 nanopillars from the scanned transmission spectra (FDTD simulation), which are shown in Figs. 4(b) and 4(c). Wherein, the simulated phase retardations $\sin(\delta/2)$ and transmission amplitude T_x of a meta-atom vs. the geometric size of its nanopillar are calculated at wavelength of 670nm. The refractive index of Poly-Si is $n = 3.25710 + i\ 0.01079$. The meta-atom has a period of 450 nm with periodic boundary condition, the nanopillar has a constant height of $h = 570$ nm. The colored dots in Figs. 4(b) and 4(c) illuminate the size of these selected geometries. The combined transmission amplitudes $T\sin(\delta/2)$ of these geometries are shown in Fig. 4(d). It can be seen from this diagram that these selected geometries present 16-step variant transmissions with a good linear relationship.

Figs. 5(a) and 5(b) show the fabricated metasurface according to the complex amplitude of the mask. The pixel sizes of the metalens are 2400 × 2400. The experiment is carried out with setup shown in Fig. 5(c). A linearly polarized beam from a diode pumped solid state laser with wavelength of 670 nm and waist of $w_0 = 1$ mm is normally incident onto the matalens, after passing through a quarter-wave plate. The subdiffraction focal field is generated at the focal plane of the metalens. We here use a microscopic measurement system consisting of a 20× objective lens, tube lens ($f = 20$ cm), and CMOS camera with a resolution of 1280 × 960 and pixel size of 3.75 μm × 3.75 μm to characterize such special fields.

Fig. 6 displays the experiment result. Where Fig. 6(a) give the transverse and Figs. 6(b) and 6(c) show the x- and y-axis intensity distributions within the field of view. As shown, the FWHMs of the experimental focus along the x- and y-axis are $w_x = 1.6\ \mu$m and $w_y = 1.2\ \mu$m, respectively. Here, we define the effective FWHM according to w_x, that is, FWHM = 0.3λ/NA. This spot size is obvious smaller than the size of the maximum spectral component, indicating the superoscillating focusing

we proposed a compact and miniaturized metalens that enables breaking the diffraction limit, and demonstrated the subdiffraction focusing capability of such metalens. Our method may open a new avenue for the design of integrated and compact devices to control the propagation of light field.

APPENDIX

Method: The dielectric metalenses were fabricated based on the process of deposition, patterning, lift off, and etching. At first, the Poly-Si film was deposited on a 500 μm-thick fused silica substrate by inductively coupled plasma enhanced chemical vapor deposition (ICPECVD), and then a 100 nm-thick Hydrogen silsesquioxane electron beam spin-on resist (HSQ, XR-1541) was spin-coated onto the Poly-Si film and baked on a hot plate at 100°C for 2 minutes. Next, the desired structures were imprinted by using standard electron beam lithography (EBL, Nanobeam Limited, NB5) and subsequently developed in NMD-3 solution (concentration 2.38%) for 2 minutes. Finally, by using inductively coupled plasma etching (ICP, Oxford Instruments, Oxford Plasma Pro 100 Cobra300), the desired structures were transferred from resist to the Poly-Si film.
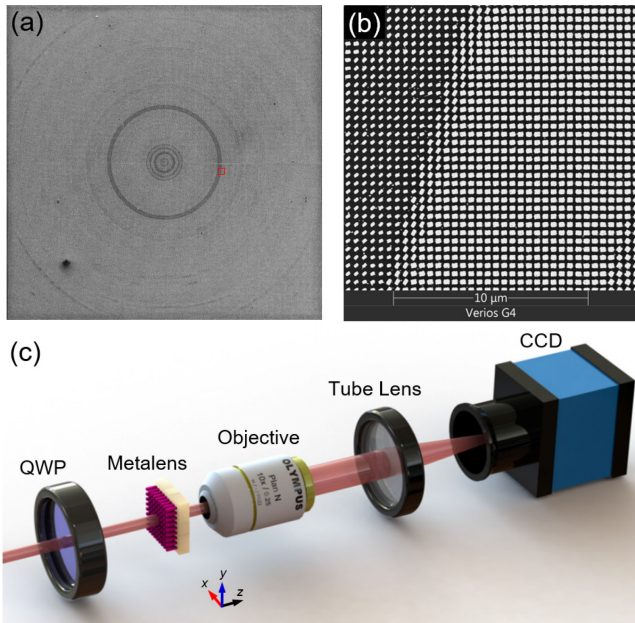

Fig. 5. (a), (b) Scanning electron microscopy image of the metalens and its locally enlarged image. The pixel sizes of the metalens are 2400 × 2400. (c) Experimental setup. QWP: quarter-wave plate. The microscopic measurement system consists of objective, tube lens, and CMOS camera.
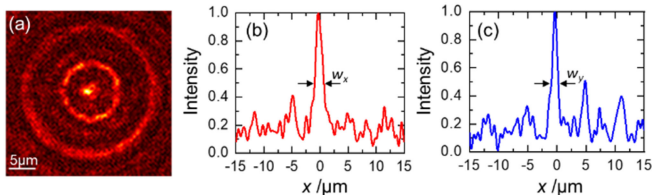

Fig. 6. (a) Transverse and (b) x- and (c) y-axis intensity distributions in the focal plane.

capability of metalens. In experiment, the total efficiency of the metalens is about 12%, which is smaller than the theoretical one because of the material absorption and overall transmission of the meta-atom [as shown in Fig. 4(d)]. In addition, we would like to note that the size of the focal spot produced by this metasurface is greater than the theoretical calculation. The reason mainly includes two aspects, first, the incident light field is Gaussian beam; second, the directly transmitted component retained due to fabrication error. Because of $T\cos(\delta/2)\neq 0$ and the lack of polarization filter, the focal field contains the directly transmitted component as a noise field.

IV. CONCLUSION

In this paper, based on the depleted Bessel beam modulation method, we introduced a dielectric subdiffraction focusing metalens that enables superoscillating focus of light field, and designed the metalens by utilizing an iteration algorithm, which depletes the central spot of a fundamental order Bessel field by overlapping first order Bessel fields. Thanks to the independent amplitude and phase control ability of dielectric metasurface,

REFERENCES

[1] U. Dürig, D. W. Pohl, and F. Rohner, "Near-field optical-scanning microscopy," *J. Appl. Phys.*, vol. 59, no. 10, pp. 3318–3327, 1986.
[2] S. W. Hell, "Far-field optical nanoscopy," *Science*, vol. 316, no. 5828, pp. 1153–1158, 2007.
[3] S. Ayas *et al.*, "Label-free nanometer-resolution imaging of biological architectures through surface enhanced Raman scattering," *Sci. Rep.*, vol. 3, no. 1, 2013, Art. no. 2624.
[4] M. Berry *et al.*, "Roadmap on superoscillations," *J. Opt.*, vol. 21, no. 5x, 2019, Art. no. 2624.
[5] G. Chen, Z.-Q. Wen, and C.-W. Qiu, "Superoscillation: From physics to optical applications," *Light: Sci. Appl.*, vol. 8, no. 1, 2019, Art. no. 56.
[6] B. K. Singh, H. Nagar, Y. Roichman, and A. Arie, "Particle manipulation beyond the diffraction limit using structured super-oscillating light beams," *Light: Sci. Appl.*, vol. 6, no. 9, 2017, Art. no. e17050.
[7] Y. Aharonov, D. Z. Albert, and L. Vaidman, "How the result of a measurement of a component of the spin of a spin-1/2 particle can turn out to be 100," *Phys. Rev. Lett.*, vol. 60, no. 14, pp. 1351–1354, 1988.
[8] M. V. Berry, "Evanescent and real waves in quantum billiards and Gaussian beams," *J. Phys. A-Math.*, vol. 27, no. 11, pp. L391–L398, 1994.
[9] M. V. Berry and S. Popescu, "Evolution of quantum superoscillations and optical superresolution without evanescent waves," *J. Phys. A-Math.*, vol. 39, no. 22, pp. 6965–6977, 2006.
[10] M. V. Berry, "A note on superoscillations associated with bessel beams," *J. Opt.*, vol. 15, no. 4, 2013, Art. no. 044006.
[11] G. Gbur, "Using superoscillations for superresolved imaging and subwavelength focusing," *Nanophotonics*, vol. 8, no. 2, pp. 205–225, 2019.
[12] F. M. Huang, N. Zheludev, Y. Chen, and F. J. G. d. Abajo, "Focusing of light by a nanohole array," *Appl. Phys. Lett.*, vol. 90, no. 9, 2007, Art. no. 091119.
[13] E. T. F. Rogers *et al.*, "A super-oscillatory lens optical microscope for subwavelength imaging," *Nat. Mater.*, vol. 11, no. 5, pp. 432–435, 2012.
[14] E. T. F. Rogers and N. I. Zheludev, "Optical super-oscillations: Subwavelength light focusing and super-resolution imaging," *J. Opt.*, vol. 15, no. 9, 2013, Art. no. 094008.
[15] Z. Wen, Y. He, Y. Li, L. Chen, and G. Chen, "Super-oscillation focusing lens based on continuous amplitude and binary phase modulation," *Opt. Exp.*, vol. 22, no. 18, pp. 22163–22171, 2014.
[16] G. Yuan, E. T. F. Rogers, and N. I. Zheludev, "'Plasmonics' in free space: Observation of giant wavevectors, vortices, and energy backflow in superoscillatory optical fields," *Light: Sci. Appl.*, vol. 8, no. 1, 2019, Art. no. 2.
[17] Y. Eliezer and A. Bahabad, "Super defocusing of light by optical suboscillations," *Optica*, vol. 4, no. 4, pp. 440–446, 2017.

[18] M. Li, W. Li, H. Li, Y. Zhu, and Y. Yu, "Controllable design of super-oscillatory lenses with multiple sub-diffraction-limit foci," *Sci. Rep.*, vol. 7, no. 1, 2017, Art. no. 1335.

[19] Y. He, Z. Wen, L. Chen, Y. Li, Y. Ning, and G. Chen, "Double-layer metallic holes lens based on continuous modulation of phase and amplitude," *IEEE Photon. Technol. Lett.*, vol. 26, no. 18, pp. 1801–1804, Sep. 2014.

[20] T. Wang, X. Wang, C. Kuang, X. Hao, and X. Liu, "Experimental verification of the far-field subwavelength focusing with multiple concentric nanorings," *Appl. Phys. Lett.*, vol. 97, no. 23, 2010, Art. no. 231105.

[21] K. Huang, H. Ye, J. Teng, S. P. Yeo, B. Luk'yanchuk, and C.-W. Qiu, "Optimization-free superoscillatory lens using phase and amplitude masks," *Laser Photon. Rev,* vol. 8, no. 1, pp. 152–157, 2014.

[22] G. Chen *et al.*, "Super-oscillatory focusing of circularly polarized light by ultra-long focal length planar lens based on binary amplitude-phase modulation," *Sci. Rep.*, vol. 6, no. 1, 2016, Art. no. 29068.

[23] F. Qin, K. Huang, J. Wu, J. Teng, C. Qiu, and M. Hong, "A supercritical lens optical label-free microscory: Sub-diffraction resolution and ultra-long working distance," *Adv. Mater.*, vol. 29, no. 8, 2017, Art. no. 1602721.

[24] Y. Liu, H. Xu, F. Stief, N. Zhitenev, and M. Yu, "Far-field superfocusing with an optical fiber based surface plasmonic lens made of nanoscale concentric annular slits," *Opt. Exp.*, vol. 19, no. 21, pp. 20233–20243, 2011.

[25] J. Yang *et al.*, "Photonic crystal fiber metalens," *Nanophotonics*, vol. 8, no. 3, pp. 443–449, 2019.

[26] D. Ploss, A. Kriesch, H. Pfeifer, P. Banzer, and U. Peschel, "Generation and subwavelength focusing of longitudinal magnetic fields in a metallized fiber tip," *Opt. Exp.*, vol. 22, no. 11, pp. 13744–13754, 2014.

[27] Z.-P. Zhuang, R. Chen, Z.-B. Fan, X.-N. Pang, and J.-W. Dong, "High focusing efficiency in subdiffraction focusing metalens," *Nanophotonics*, vol. 8, no. 7, pp. 1279–1289, 2019.

[28] X. Guo *et al.*, "On-demand light wave manipulation enabled by single-layer dielectric metasurfaces," *APL Photon.,* vol. 6, no. 8, 2021, Art. no. 086106.

[29] J. Li *et al.*, "Simultaneous control of light polarization and phase distributions using plasmonic metasurfaces," *Adv. Funct. Mater.*, vol. 25, no. 5, pp. 704–710, 2015.

[30] D. Tang *et al.*, "Ultrabroadband superoscillatory lens composed by plasmonic metasurfaces for subdiffraction light focusing," *Laser Photon. Rev.*, vol. 9, no. 6, pp. 713–719, 2015.

[31] G. Yuan, K. S. Rogers, E. T. F. Rogers, and N. I. Zheludev, "Far-field superoscillatory metamaterial superlens," *Phys. Rev. Appl.*, vol. 11, no. 6, 2019, Art. no. 064016.

[32] W. Li, Y. Yu, and W. Yuan, "Flexible focusing pattern realization of centimeter-scale planar super-oscillatory lenses in parallel fabrication," *Nanoscale*, vol. 11, no. 1, pp. 311–320, 2019.

[33] Z. Wu *et al.*, "Broadband dielectric metalens for polarization manipulating and superoscillation focusing of visible light," *ACS Photon.*, vol. 7, no. 1, pp. 180–189, 2020.

[34] V. V. Kotlyar, S. S. Stafeev, A. G. Nalimov, and L. O'Faolain, "Subwavelength grating-based spiral metalens for tight focusing of laser light," *Appl. Phys. Lett.*, vol. 114, no. 14, 2019, Art. no. 141107.

[35] W. Chen *et al.*, "Generation of wavelength-independent subwavelenght bessel beams using metasurfaces," *Ligth Sci. App.*, vol. 6, no. 5, 2017, Art. no. e16259.

[36] Y.-X. Shen *et al.*, "Ultrasonic super-oscillation wave-packets with an acoustic meta-lens," *Nat. Commun.*, vol. 10, no. 1, 2019, Art. no. 3411.

[37] X. Dai *et al.*, "Holographic super-resolution metalens for achromatic sub-wavelength focusing," *ACS Photon.*, vol. 8, no. 8, pp. 2294–2303, 2021.

[38] X. Guo *et al.*, "Tying polarization-switchable optical vortex knots and links via holographic all-dielectric metasurfaces," *Laser Photon. Rev.*, vol. 14, no. 3, 2020, Art. no. 1900366.

[39] Z. Wu, H. Deng, X. Li, L. Xiong, L. Shang, and G. Chen, "Superoscillatory metalens for an azimuthally polarized wave with different orbital angular momentum," *Opt. Eng.*, vol. 59, no. 9, 2020, Art. no. 090501.

[40] T. Li *et al.*, "Generation and conversion dynamics of dual bessel beams with a photonic spin-dependent dielectric metasurface," *Phys. Rev. Appl.*, vol. 15, no. 1, 2021, Art. no. 014059.

[41] K. Huang *et al.*, "Planar diffractive lenses: Fundamental, functionalities, and applications," *Adv. Mater.*, vol. 30, no. 26, 2018, Art. no. 1704556.

[42] Y. Kozawa, D. Matsunaga, and S. Sato, "Superresolution imaging via superoscillation focusing of a radially polarized beam," *Optica*, vol. 5, no. 2, pp. 86–92, 2018.

[43] K. S. Rogers, K. N. Bourdakos, G. H. Yuan, S. Mahajan, and E. T. F. Rogers, "Optimising superoscillatory spots for far-field super-resolution imaging," *Opt. Exp.*, vol. 26, no. 7, pp. 8095–8112, 2018.

[44] Z. Wu *et al.*, "Optimization-free approach for generating sub-diffraction quasi-non-diffracting beams," *Opt. Exp.*, vol. 26, no. 13, pp. 16585–16599, 2018.

[45] X. H. Dong, A. M. H. Wong, M. Kim, and G. V. Eleftheriades, "Superresolution far-field imaging of complex objects using reduced superoscillating ripples," *Optica*, vol. 4, no. 9, pp. 1126–1133, 2017.

[46] T. Zacharias, B. Hadad, A. Bahabad, and Y. Eliezer, "Axial sub-Fourier focusing of an optical beam," *Opt. Lett.*, vol. 42, no. 16, pp. 3205–3208, 2017.

[47] X. Fan *et al.*, "Axially tailored light field by means of a dielectric metalens," *Phys, Rev. Appl.*, vol. 14, no. 2, 2020, Art. no. 024035.

[48] X. Guo *et al.*, "Full-color holographic display and encryption with full-polarization degree of freedom," *Adv. Mater.*, vol. 34, 2022, Art. no. 2103192.